THE JOURNAL OF PHYSICAL CHEMISTRY B

ARTICLE

pubs.acs.org/JPCB

Assembly of Polyethyleneimine in the Hexagonal Mesophase of Nonionic Surfactant: Effect of pH and Temperature

Kamendra P. Sharma,[†] Chandan Kumar Choudhury,[‡] Sonal Srivastava,[§] H. Davis,[∥] P. R. Rajamohanan,[∥] Sudip Roy,[‡] and Guruswamy Kumaraswamy*[,†]

[†]Complex Fluids and Polymer Engineering Group, Polymer Science and Engineering Division, National Chemical Laboratory, Pune, India

[‡]Physical Chemistry Division, National Chemical Laboratory, Pune, India

[§]Chemical Engineering Department, IIT Kharagpur, India

[∥]NMR Center, National Chemical Laboratory, Pune, India

Supporting Information

ABSTRACT: We investigate the dispersion of a pH responsive polymer, polyethyleneimine, PEI, in a hexagonal (H_1) mesophase of a nonionic surfactant, $C_{12}E_9$, and water, at pH ranging from basic (pH = 12.8) to acidic (pH = 1). While the $C_{12}E_9/H_2O$ phase behavior is independent of pH, we demonstrate that, in the PEI/$C_{12}E_9/H_2O$ system, changing the pH influences PEI-$C_{12}E_9$ interactions, and thus, influences the isotropic-H_1 phase transition. With decrease in pH, there is increasing protonation of the PEI chain, and consequently, the chain extends. We show, using a combination of SAXs, optical microscopy and visual experiments, that the inclusion of PEI in a 1:1 surfactant−water mixture, lowers the hexagonal-isotropic transition temperature, T_{HI}. At higher pH = 12.8, T_{HI} shows a pronounced decrease from 50 to 13 °C on addition of PEI, and the PEI/$C_{12}E_9/H_2O$ system forms a transparent gel. At pH = 1, we observe qualitatively different behavior and an opaque gel forms below T_{HI} = 25 °C. The isotropic-H_1 transition, in turn, influences the phase separation of PEI chains from the $C_{12}E_9/H_2O$ system. 2D NMR ROESY data provides evidence that there are strong surfactant−PEI interactions at high pH that significantly reduce at lower pH. The NMR data is in accord with molecular dynamics simulations that show that surfactants strongly aggregate with unprotonated PEI chains, but not with fully protonated chains; thus, in this system, the pH controls a cascade of microstructural organization: increasing pH decreases chain protonation and increases polymer−surfactant interactions, resulting in suppression of the isotropic-H_1 transition to lower temperatures, thus, influencing the phase separation of PEI from the surfactant/water system.

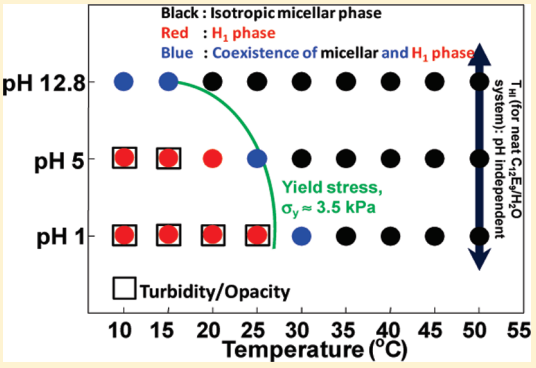

INTRODUCTION

Organized surfactant mesophases are increasingly finding applications as matrices for sustained release of therapeutic molecules[1] and in the foods and cosmetics industry.[2] Often, the active compounds to be delivered are complexed with polymers that either stabilize the compound or that play a role in targeted delivery. For example, polyethyleneimine (PEI) is widely used to prepare polymer complexes for pharmaceutical formulations in gene transfection, drug delivery, and so on.[3−6] When polymer complexes need to be incorporated in a surfactant matrix, it is important to understand the nature of the interactions between the polymer and the surfactant. Such interactions might be influenced by the external environment, namely, pH, temperature, and so on. Recently, we have demonstrated[7] that, for a thermo-responsive polymer, PNIPAM, dispersed in a nonionic surfactant/water system, the phase of the matrix, rather than the chemistry, controls the polymer volume transition. Here, we investigate the microstructure, and interactions when a pH responsive polymer, PEI, is dispersed in nonionic surfactant, $C_{12}E_9$/water system that can form a hexagonal mesophase (H_1).

There is extensive literature on investigations of colloidal mixtures of polymers and surfactants due to the technological importance of such systems in industrial and biological applications.[8] Charged polymers associate strongly with oppositely charged surfactants through electrostatic interactions.[9] Interactions between like-charged polymers and surfactants are repulsive; however, even in such systems, the surfactants might associate with the polymer through hydrophobic interactions, especially if the polymer has long alkyl side chains.[10] Interactions between a charged polymer and nonionic surfactants are typically weak, relative to charged polymer−charged surfactant interactions. Charged polymers can associate with nonionic surfactants through H-bonding or through hydrophobic interactions.[11,12]

Received: March 20, 2011
Revised: June 21, 2011
Published: June 22, 2011

Most of the literature on PEI-surfactant complexes focuses on interactions of sodium dodecyl sulfate (SDS), an anionic surfactant, with linear and branched PEI.[13−15] For example, Wang et al.[15] reported the pH dependent association of linear and branched PEI, with SDS below its critical micellization concentration. At low pH, linear PEI is highly protonated and therefore interacts strongly with SDS. At higher pH (=10), the PEI behaves as a neutral polymer and therefore SDS remains associated only as adsorbed spherical micelles. The PEI chain structure has also been shown to play a role, with branched PEI associating more strongly at all pH values compared to linear chains. Gainanova et al.[16] reported that modified PEI−nonionic surfactant complexes formed at very low surfactant concentrations in chloroform showed catalytic activity toward the phosphorylation reaction. This catalytic activity is inhibited as the surfactant concentration is increased above the critical association concentration.

Research on polymers in surfactant mesophases[17] has focused mainly on lamellar surfactant phases, due to their morphological similarity with biological membranes. As the interactions between lipid membranes and their associated membrane proteins are known to modulate protein structure and function, polymers represent simple model systems to investigate conformational changes on associating with lamellar phases. Polymer−surfactant interactions determine polymer chain localization, for example, polymer chains might be localized in the water region,[18] within the membrane,[19] partitioned between the aqueous phase and the membrane,[20] or stay adsorbed on the surface of the membrane due to hydrophobic interactions.[21] Polymer localization is also a function of the size of the polymer chain, relative to the interlamellar spacing. For polymers in lamellar bilayer phases, low molecular weight polymers are accommodated in and swell the lamellar phase, while high molecular weight polymers are excluded from the lamellar phase.[22] Typically, surfactant lyotropic lamellar mesophases have a repeat distance ranging from 2 to 10 nm, and polymers having a coil size in this range are typically accommodated in the surfactant mesophase. Pacios et al.[23,24] investigated dispersions of a noninteracting polymer, poly(dimethylacrylamide), in the lamellar mesophase of anionic surfactant, AOT. Their work suggests that the lamellar mesophase acts as a "sieve" that can "dissolve" polymer chains with a chain size smaller than or similar to the dimensions of the water channel, d, and that the mesophase expels larger chains. Therefore, the authors suggest that confinement of noninteracting polymers in the lyotropic liquid crystal largely depends on the size/geometry of the polymer chain. Similarly, it has been observed[22] that high molecular weight carbohydrates are expelled from the lamellar phase of a zwitterionic phospholipid, lecithin, and remain dispersed in the isotropic phase. However, Ligoure et al.[25] have reported confinement of a high molecular weight noninteracting poly(vinylpyrollidone) having dimensions much larger than the lamellar phase repeat spacing. They suggested that confinement of the high molecular weight polymer was a result of intermembrane repulsive interactions that could be controlled by changing the ionic strength. We also mention in passing that there is considerable literature on dispersion of colloidal particles in lamellar surfactant phases.[26] However, the entropic consequences of conformational changes of solvated polymer chains on confinement in a surfactant mesophase, result in different behavior as compared to particles.

Association of nonionic surfactants with hydrophobically modified polymers has also been reported. Iliopoulos and Olsson[27] used a combination of viscosity and self-diffusion measurements to report the association of hydrophobically modified poly(sodium acrylate) with the micelles and lamellar phase of $C_{12}E_5$ and of $C_{12}E_8$. They report polymer−surfactant association as a result of hydrophobic interactions between the alkyl side chains of the polymer and the alkyl tails of the surfactants and suggest that the polymer chains adsorb on the surface of the surfactant lamellae. Similar results were shown by Yang et al.[28] for hydrophobically modified poly(sodium acrylate) in the lamellar and sponge phases of $C_{12}E_5$. Interactions between a random heteropolymer, poly(styrene- sodium styrene sulfonate), of 25000 $g\cdot mol^{-1}$ molecular weight, and a lamellar phase of a nonionic surfactant has also been studied as a function of charge content on the polymer.[29,30] A lamellar phase formed at high surfactant to water ratio, was observed to exist until high concentration of polymer, independent of the extent of charge on the polymer. An increase in water content leads to a first order phase transition to a cubic phase.

There are comparatively few reports of polymers[1f,g,7] in hexagonal phases, even though such mesophases are now being used[1b] as matrices for controlled release. In this work, we use a combination of experimental techniques and molecular simulations to probe the effect of pH on PEI−nonionic surfactant interactions, and therefore, on the isotropic-H_1 phase transition. We begin with a detailed description of the experimental system and then present experimental results, followed by simulation data.

EXPERIMENTAL SECTION

Materials. PEI was obtained from Sigma Aldrich and was used as received (M_w = 2000 $g\cdot mol^{-1}$ and M_n = 1800 $g\cdot mol^{-1}$, as reported by the manufacturer). Nitric acid, HNO_3, used to adjust the pH of the sample, was obtained from Merck as a 70% (w/v) solution. Hydrochloric acid, HCl was obtained as 35−38% aqueous solution from SD-Fine chemicals. Nonaethyleneglycol dodecyl ether, $C_{12}E_9$, nonionic surfactant was obtained from Sigma and used as obtained. We note that C_nE_m surfactants are typically prepared by ethoxylation of alkyl alcohols and are typically comprised of a mixture of polydisperse ethylene oxide blocks. These chemical variations result in bottle-to-bottle differences in the measured isotropic−hexagonal transition temperature (T_{HI}; Supporting Information, Figure S0). While such variations do not qualitatively change our conclusions, we ensured that all the experiments reported here were performed using surfactant from the same bottle.

Samples were prepared by mixing surfactant, PEI, and water at 50 °C in the low viscosity isotropic micellar phase and then cooling down to room temperature. The 50% PEI solution from the manufacturer was directly used to prepare samples at pH = 12.8. For lower pH samples, the stock solution of PEI was diluted with water and the pH was adjusted by adding 70% (w/v) HNO_3. Samples were prepared such that the ratio of surfactant to water in the final sample was always 1:1 by weight. The pH of the samples was checked using a Mettler Toledo instrument (SevenMulti) calibrated with standards. Our system represents a model, to understand the pH-dependent behavior of PEI in a nonionic surfactant mesophase.

Sample Preparation for NMR. Samples were prepared for NMR, with D_2O as the solvent, using the following procedure. A known amount of stock solution (50% by weight) of PEI was first rota-vaporized at 70 °C for 1 h. After this, the sample was frozen using liquid N_2 and then lyophilized (Heto PowerDry LL3000) at −55 °C for 24 h. This procedure resulted in a PEI sample with a concentration of 99 wt %. We were unable to dry the sample any

further, even after repetition of the above procedure. The sample at pH 12.8 was directly prepared by diluting the concentrated PEI solution to 5 wt % using D_2O as the solvent. For lower pH samples, the concentrated PEI solution was first diluted with D_2O until the concentration reached 15 wt % and then it was subjected to change in pH by adding required amount of concentrated, 70% (w/v) HNO_3. Finally, the concentration was adjusted to 5 wt % with D_2O. Thus, all the samples prepared for NMR studies contained H_2O that could not be removed during the concentration of PEI and also from the HNO_3. Samples containing 25 wt % surfactant and 5 wt % PEI for 2D ROESY experiments were prepared in a similar manner as mentioned above. We note here that the pH reported is measured using an electrode calibrated using $[H^+]$. Thus, it is more appropriate to term this pH*, namely, the *measured* value of pH obtained using an electrode calibrated with $[H^+]$ for samples containing H_2O/D_2O. However, for convenience, we refer to this as pH in our manuscript. We have measured the ^1H NMR spectra for solutions of PEI in H_2O and in H_2O/D_2O under conditions of identical *measured* pH and find that there are only minor differences between the spectra (Supporting Information).

Characterization Tools. NMR studies were done on (1) aqueous solution of PEI at different pH and (2) mixtures of PEI/$C_{12}E_9$/H_2O at different pH. All NMR measurements were performed on a Bruker AV400 MHz spectrometer operating at 400 and 100 MHz, respectively, for ^1H and ^{13}C using a 5 mm BBFO probe. For 2D ROESY measurements, a standard 2D pulse sequence with a spin lock (CW) time of 200 ms was used.[31] 2D data containing 256 increments were collected by adding 16 transients with a repetition delay of 3 s using 1 K data points.

Small angle X-ray scattering (SAXs) was used to obtain the phase behavior of 1:1 $C_{12}E_9/H_2O$ mixture in the presence of PEI. The scattering experiments were carried out on a three pinhole collimated Bruker Nanostar machine equipped with rotating copper anode, operating at 45 kV and 100 mA and providing characteristic K_α radiation of wavelength 1.54 Å. The experiments were performed in the normal resolution mode having a q-range of 0.011−0.2 $Å^{-1}$. The samples were filled in a 2 mm (outer diameter) glass capillary having a wall thickness of ∼10 μm and scanned at temperatures from 10 to 50 °C. The temperature was controlled using a Peltier stage controlled by a MCU-temperature controller. The scattered data was collected using a 2-D Histar detector and was later converted from 2-D to 1-D by azimuthal averaging using the Bruker software. Optical Microscopy was performed on an Olympus BX-50 microscope equipped with a Lookman camera. Viscosity measurements were performed on a Ubbelohde viscometer having diameter of 0.53 mm mounted on a Schott instrument.

Computational Procedure. We have performed an all atomistic molecular dynamics simulation of (a) a linear 20-mer and 50-mer polyethyleneimine (PEI, -(CH_2-CH_2-NH)-) in water and (b) 10 linear 20-mer PEI chains with 49 surfactant molecules and water using Gromacs 4.0.7.[32] We note that the 50-mer PEI has approximately similar molecular weight when compared with the polymer used for the experimental study. Results from the simulation of 20-mer PEI were compared with the results of Ziebarth et al.[33] to validate our simulations. All the simulations in the present study were performed with the amber force field.[34] As in Ziebarth et al.,[33] the PEI chains had three subsystems on the basis of different levels of protonation, namely, no protonation (representative of behavior at high pH, basic medium), protonation on every alternate nitrogen atom along the chain (representative of intermediate pH), and complete protonation (representative of very low pH, acidic medium). We have presented data for 50-mer PEI simulations for these three subsystems. For the PEI−surfactant systems, we simulated only the nonprotonated and all-protonated PEI. Protonation was done at the secondary nitrogen atoms present in the polymer chain. The partial charges for each atom were derived from quantum chemical calculations using the Gaussian 09 package[35] with 6-31G* basis sets and the CHELPG method.[36] The derivation of the charges was necessary because the amber force field did not contain the partial charges of the atom types involved in the present study. All the other parameters (bonded, Lennard-Jones parameters) were adopted from the amber force field itself, as in Ziebarth et al.[33] The charges for each atom type used for the simulation of all the systems are summarized in the Supporting Information (Table S1). The TIP3P water model[37] was used in all simulations. The 20-mer and 50-mer systems had a single chain solvated with a TIP3P water model, while the PEI−surfactant system consisted of 10 20-mer PEI chains along with 49 surfactant molecules and 6125 and 5887 water molecules for nonprotonated and all-protonated systems, respectively. The charges for the surfactant atoms were adapted from the OPLS-AA force field. The protonated nitrogen atoms were neutralized using chloride ions, as force fields for nitrate ions were not available. We have confirmed that the concentration dependence of the viscosity of PEI solutions at different values of pH does not depend on whether nitric or hydrochloric acid is used to adjust the pH (see Supporting Information, Figure S1). Therefore, we believe that the trends from the simulation data (obtained using a chloride counterion) may be compared with the experimental data (where nitric acid was used to adjust the pH). The time step of integration in our simulations was 0.001 ps for every system. The electrostatic and nonbonded potential cutoff was 1.2 nm and Particle-Mesh Ewald[38] was used to take care of the electrostatic interactions. Simulations were carried out at 300 K for a 50 ns production run for PEI single chains in water and at 400 K for a 100 ns production run for the PEI−surfactant systems (NPT ensemble using Berendsen barostat[39] with time constant of 1.0 ps and v-rescale temperature coupling[40] with time constant of 0.100 ps). The trajectory was recorded after every 2 ps. Simulations during pre- and postequilibration (5 ns of simulation) were not included for our analysis.

RESULTS

Our results are organized as follows: we first describe the effect of pH on the aqueous solution of PEI and on the surfactant/water system. We then examine the influence of adding PEI to the surfactant/water system and use a combination of visual observations, microscopy, SAXs, and NMR to understand the pH-dependent changes in surfactant−PEI interactions. Finally, we present simulation results that provide a molecular understanding of our experimental observations.

Aqueous Solutions of PEI. There is a qualitative change in the ^1H NMR of a dilute (5%, weight/weight) solution of PEI (in D_2O) with change in pH (Figure 1a−c). At pH 12.8 (Figure 1a), there are multiple peaks between δ = 2.45−2.70 that can be attributed to the -CH_2- protons adjacent to nitrogen atoms. Protons on nitrogen atoms are rapidly exchanged with deuterium from the solvent, D_2O, and are, therefore, not detected. Multiple peaks are observed for -CH_2- protons due to the heterogeneity in the environment experienced by the nuclei of these protons. In PEI, this heterogeneity can result either from partial protonation of the chain (viz., protonation of only some amine groups) or

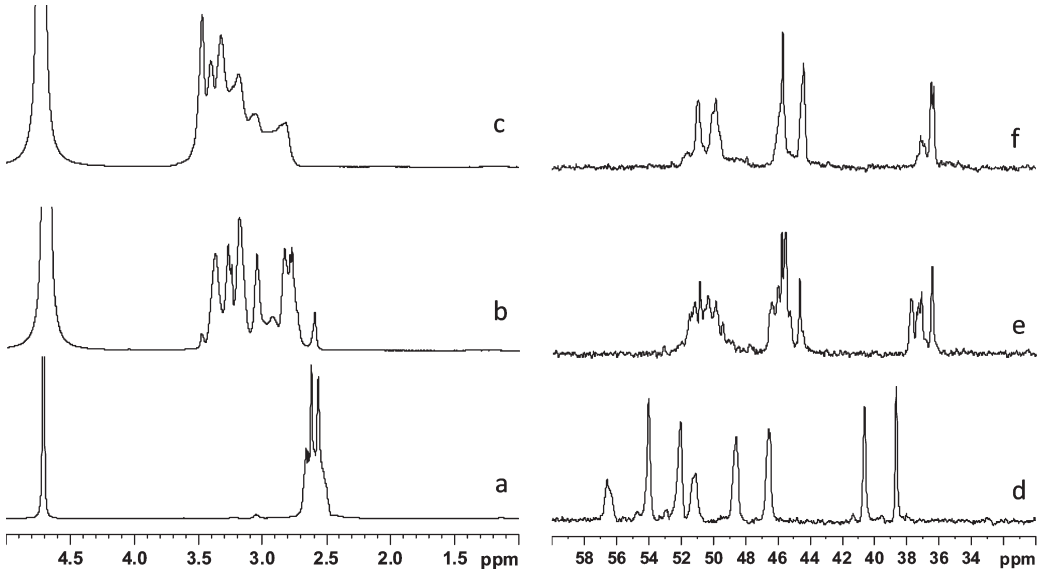

Figure 1. ^{1}H NMR of 5 wt % PEI in D_2O at (a) pH 12.8, (b) pH 5, and (c) pH 1. ^{13}C NMR of the same sample at (d) pH 12.8, (e) pH 5, and (e) pH 1.

from branching along the chain.[41] As the pK_a values for the primary, secondary, and tertiary amines range from 8.2 to 9.5,[33] it is unlikely that any of the amine groups will be protonated at a pH = 12.8. However, the presence of primary, secondary, and tertiary amines due to branching along the PEI chain results in a heterogeneous environment for the non-nitrogen atoms. For example, protons on carbon atoms in the α-position to a nitrogen from a tertiary amine are more deshielded relative to a secondary and primary amine.[41] Thus, we believe that it is branching along the PEI chain that results in multiple peaks for the -CH_2- protons at pH = 12.8 (Figure 1a). Our results are in accord with studies reported in the literature.[42]

As the pH of the PEI is reduced to 5, the -CH_2- protons show peaks between δ = 2.55−3.50, namely, downfield relative to those observed for pH 12.8 (compare Figure 1b with 1a). At this pH, we expect that the amine groups along the PEI chain get protonated, thus, deshielding the protons on carbons that are α and β to the nitrogen atoms. We observe a larger number of peaks at pH = 5 relative to pH = 12.8, suggesting a greater inhomogeneity in the environments for the protons. We attribute this to partial protonation of the amine groups at this pH, resulting in a distribution of charge along the PEI chain. At the lowest pH (=1, Figure 1c), we anticipate further protonation of the amine groups on the PEI. This results in a shift of the methylene proton signals to δ = 2.55−3.60, downfield relative to that at pH = 5. Interestingly, there are fewer -CH_2- proton peaks relative to pH = 5, suggesting that most of the amines are protonated at this low pH and, consequently, there is less heterogeneity in the proton environments. We observe a larger number of -CH_2- proton peaks at pH 1, relative to at pH 12.8, suggesting that, even at this low pH, the amine groups on the PEI are not completely protonated. This is in agreement with the literature, where it has been reported only ∼70% amines in PEI can be protonated due to conformational effects.[43]

The effect of protonation is more clearly visible in the ^{13}C spectra (Figure 1d−f). At pH 12.8, we observe eight signals that we classify into three categories (Figure 1d). The more deshielded signals (δ = 57−52 ppm) correspond to the methylene carbon attached to the tertiary nitrogen. The three signals following them (δ = 51.5−46 ppm) represent methylenes attached to the secondary amine group (-NH-). The remaining signals (most shielded, δ = 41−38 ppm) are attributed to the methylene carbon bonded to the terminal primary amino groups.[41] Assuming that none of the amines on the PEI are protonated, we can estimate that the ratio of tertiary, secondary, and primary amines from the ^{13}C NMR is 43:37:20. We note here that, to quantitate the ratio of tertiary/secondary/primary amines, the ^{13}C NMR spectrum was collected with adequate time for relaxation and without the nuclear Overhauser effect. The spectrum at pH 5 exhibited shielding of all the resonances indicating random ionization of most of the amine functionalities present in PEI (Figure 1e). Reducing the pH further to 1 (Figure 1f) did not induce any further shielding, but led to broadening of signals, especially in the 52−48 ppm region (associated with the protonated secondary amine functionalities and protonated/non protonated tertiary amine functionalities; the observed broadening might arise[41] due to protonation of the amines, and scalar coupling with the ^{14}N spin, as well as "unfavorable" relaxation processes, possibly due to shortening of T_2). As with the proton NMR, we observe a decrease in the number of peaks relative to that at pH = 5, indicating that protonation of most of the amine groups results in a decrease in heterogeneity in the chemical environments.

PEI in the Presence of $C_{12}E_9/H_2O$ at Different pH and Temperature. There is no effect of pH on the isotropic-H_1 phase transition of the 50/50 $C_{12}E_9/H_2O$ system (Supporting Information, Figure S2). This is as expected, since $C_{12}E_9$ is a nonionic surfactant. For this system, the H_1 phase forms a transparent gel below the isotropic-H_1 transition temperature, T_{H1}, ≈50 °C at all pH values between 1 and 12.8. The fan-like texture and domain size observed in the optical microscopy is also independent of pH in this range. However, on addition of PEI, we see a dramatic influence of pH on the behavior of the 5% PEI−47.5% $C_{12}E_9$−47.5% water, which we examine in detail in this section. We report our results at pH = 12.8, 5, and 1.

Visual Observations. At high temperature, namely, above 50 °C, a 5 wt % PEI sample in 47.5/47.5 wt % of $C_{12}E_9/H_2O$ is a transparent solution of low viscosity for all three pH values

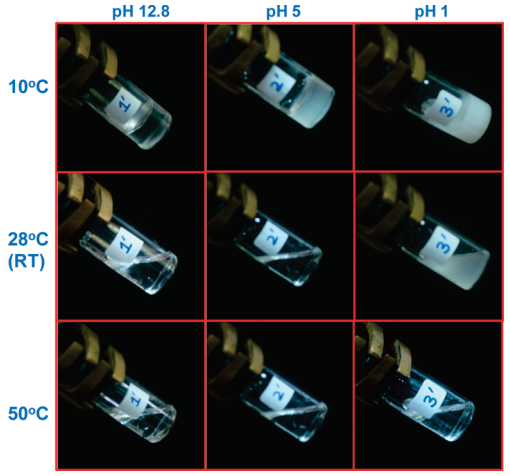

Figure 2. Temperature-dependent visual observations for 5 wt % PEI in 47.5/47.5% (by weight) of $C_{12}E_9/H_2O$ at three different pH values of 12.8, 5, and 1. The vial was tilted in the photograph so that the formation of a self-standing gel is apparent.

examined (Figure 2, bottom row), similar to the neat $C_{12}E_9/H_2O$ system. However, samples containing PEI were not observed to gel on cooling to just below T_{HI} for the neat $C_{12}E_9/H_2O$ system, (≈50 °C). For pH = 12.8, the PEI/$C_{12}E_9/H_2O$ sample was a transparent, low viscosity solution even at room temperature (≈28 °C, Figure 2, first column, middle). We observed a noticeable increase in viscosity only on cooling to ∼16 °C, and the sample became a self-standing clear gel at ∼13 °C. At 10 °C (Figure 2, first column, top), the PEI/$C_{12}E_9/H_2O$ sample at pH = 12.8 was a transparent gel. We now examine the behavior of the PEI/$C_{12}E_9/H_2O$ sample at pH = 5. At pH = 5, the sample was a clear low viscosity solution on cooling to room temperature (∼28 °C, Figure 2, second column, middle). However, on cooling to ∼25 °C (Figure S3a), the sample formed a transparent gel. On further cooling to ≈17 °C, this gel turned turbid (Figure S3b) and we observed a progressive increase in opacity of the sample until 13 °C. We could observe no further change on cooling to 10 °C (Figure 2, second column, top). In contrast to the higher pH sample, at pH = 1, the sample containing 5% PEI turned turbid but did not gel at room temperature, ∼28 °C (Figure 2, third column, middle), and then transformed into an opaque gel on cooling to ∼25 °C (Figure S4). The sample showed no further change to the eye, on cooling to 10 °C (Figure 2, third column, top). We now relate our visual observations to the sample microstructure probed using SAXs and optical microscopy.

Small Angle X-ray Scattering Studies. Small angle X-ray scattering (SAXs) was performed on PEI/$C_{12}E_9/H_2O$ samples at all three values of pH, as a function of temperature (Figure 3), and can be compared with measurements on the neat $C_{12}E_9/H_2O$ sample (Supporting Information, Figure S2). In the neat $C_{12}E_9/H_2O$ sample, hexagonal order in the H_1 phase is characterized by peaks in the SAXs scattering at $q \sim 0.11$ Å^{-1} and 0.18 Å^{-1} ($\approx 0.11 \times \sqrt{3}$) at temperatures below T_{HI}. On heating above T_{HI} (above 50 °C), a broad peak is observed at $q \sim 0.105$ Å^{-1} that characterizes the isotropic micellar phase.

At pH = 12.8, for the 5% PEI sample, we observe a broad micellar peak at $q \sim 0.1$ Å^{-1} at 50 °C (Figure 3a) that shifts to higher q values when the temperature is decreased. Bragg peaks characterizing the H_1 phase appear at 15 °C (primary peak

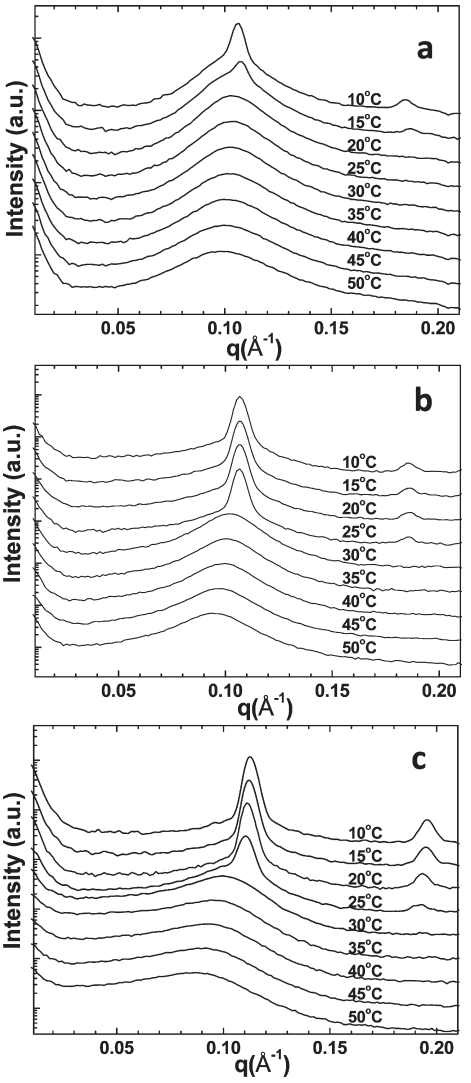

Figure 3. Temperature-dependent SAXs spectra of 5% PEI in 47.5/47.5 wt % of $C_{12}E_9/H_2O$ system at (a) pH 12.8, (b) pH 5, and (c) pH 1.

position ≈0.11 Å^{-1}; second order peak ≈0.19 Å^{-1}), namely, in accord with the temperature at which a self-standing gel is observed to form. However, the H_1 Bragg peak at 15 °C exhibits a shoulder on the low q side, suggesting coexistence of the isotropic micellar phase. On decreasing the temperature to 10 °C, we observe that the H_1 peaks become more pronounced, suggesting an increase in the fraction of and improved ordering in the H_1 phase. We also note a small apparent shift in the position of the H_1 peaks to lower q values on cooling from 15 to 10 °C that might result from the change in fraction of the isotropic micellar phase (primary peak appears to shift from $q \approx 0.11$ to 0.107 Å^{-1} from 15 and 10 °C, respectively; reproducibility in peak position = ±0.002 Å^{-1}).

At pH = 5 (Figure 3b), SAXs from the sample shows the broad isotropic micellar peak at 50 °C and H_1 peaks are observed on cooling to 25 °C (primary peak $q \sim 0.11$ Å^{-1} with second order peak at $q \sim 0.18$ Å^{-1}). Thus, in accord with our visual observations, T_{HI} for the PEI/$C_{12}E_9/H_2O$ sample at pH = 5, is between 30 and 25 °C. With a further decrease in temperature below T_{HI}, the H_1 peaks grow more prominent, as for the sample at pH = 12.8. Similarly, for the PEI/$C_{12}E_9/H_2O$ sample at pH = 1

dx.doi.org/10.1021/jp202614x |J. Phys. Chem. B 2011, 115, 9059–9069

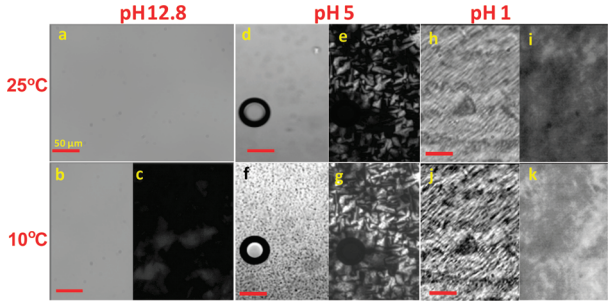

Figure 4. Optical micrographs of 5 wt % PEI in 47.5/47.5% (by weight) $C_{12}E_9/H_2O$ system. Scale bar for the micrographs at pH 1 and pH 12.8 is 50 μm, whereas for pH 5, the scale bar is 25 μm. Images between parallel polarizers are presented in (a), (b), (d), (f), (h), and (j), and the corresponding micrographs between crossed polarizers are presented in (c), (e), (g), (i), and (k), respectively.

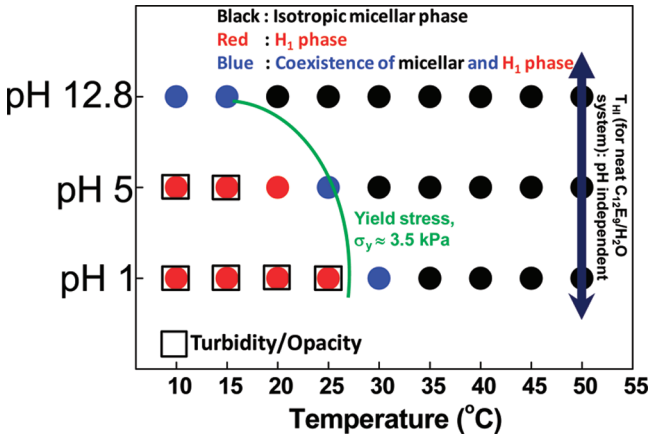

Figure 5. State diagram based on visual, SAXs, and optical microscopy studies. The green line represents the temperatures above which the samples yield.

(Figure 3c), we can observe a transition from an isotropic micellar state (characterized by a broad peak $q \sim 0.09$ Å^{-1}) on cooling from 50 to 25 °C, where peaks from the H_1 phase appear (at $q \approx 0.11$ and ≈ 0.19 Å^{-1}). The H_1 peaks grow more prominent on cooling, and we cannot clearly observe the broad peak from the isotropic micellar phase below 25 °C. Our SAXs measurements are in accord with the visual observations: T_{HI} from SAXs match the gelation temperatures from our visual observations. Thus, for the PEI/$C_{12}E_9/H_2O$ samples, formation of an H_1 phase appears to be inhibited at higher pH: T_{HI} decreases with an increase in pH, and when the H_1 phase forms, the SAXs peaks that characterize it are significantly broadened at higher pH.

Optical Microscopy Studies. We now present optical microscopy images of our samples observed between parallel, as well as, crossed polarizers, as a function of pH and temperature (Figure 4). The neat H_1 phase (viz., not containing PEI) shows a fan-like texture that is characteristic of the hexagonal phase, when observed between crossed polarizers (see, for example, images in ref 44). At 45 °C, the PEI/$C_{12}E_9/H_2O$ samples are transparent at pH between 1 and 12.8, and are in the isotropic micellar phase. Therefore, optical microscopy of these samples does not yield any information; a uniform, featureless image is observed between parallel polarizers and no light is transmitted through crossed polarizers (Supporting Information, Figure S5). At pH = 12.8, the H_1 phase does not form at25 °C and, therefore, we can obtain no information from optical microscopy, as in the case of the samples at 45 °C (Figure 4a). However, on cooling to 15 °C, a birefringent fan-like texture, characteristic of the H_1 phase, is observed between crossed polarizers (the image at 10 °C, is shown in Figure 4c). The corresponding image between parallel polarizers (Figure 4b) is uniform, suggesting that there is no aggregation of PEI. In contrast to the sample at pH = 12.8, the behavior is different at lower pH.

At pH = 5, the H_1 phase forms at around 26 °C and the characteristic fan like texture is visible in the image between crossed polarizers at 25 °C (Figure 4e). The corresponding image, between parallel polarizers (Figure 4d), has no features. These images accord with our visual observation (Figure 2, second column, middle, and Figure S3a) that the sample remains transparent at 25 °C, after the formation of the H_1 phase. However, on cooling, the sample turned turbid at around 17 °C (Figure S3b). When viewed under the microscope at 10 °C, we observe the formation of optically dense structures that are a few micrometers in size (Figure 4f) and that are localized at the boundaries of the H_1 phase domains. The formation of these structures that we expect will scatter visible light correlates with the onset of turbidity in the sample. We also note that the domain structure of the H_1 phase (Figure 4g) formed at 25 °C does not change with the formation of these structures. We had previously reported[7] that, for poly(*N*-isopropylacrylamide) (PNIPAM) chains in the $C_{12}E_9/H_2O$ system, we observe the precipitation of PNIPAM from the surfactant/water phase once an H_1 phase forms. Further, the PNIPAM was observed to be localized at the domain boundaries of the H_1 domain. Similarly, in the PEI/$C_{12}E_9/H_2O$ system investigated here, we believe that the structures that are observed in the optical microscopy are formed by precipitation of PEI chains that phase separate from the $C_{12}E_9/H_2O$ to form micrometer sized aggregates. These polymer aggregates cannot be accommodated in the H_1 phase and are expelled to the boundaries of the H_1 domains.

At lower pH, namely, for the sample at pH = 1, we observe the formation of droplets that phase separate from the isotropic micellar phase, at about 28 °C (image between parallel polarizers, Supporting Information, Figure S6). These droplets scatter light, rendering the sample opaque. On cooling the sample to around 26 °C, the fan like texture characteristic of the H_1 phase is observed between crossed polarizers. This fan like texture is clearly visible at 25 °C (Figure 4i). Between parallel polarizers, we observe that the droplets that phase separate at 28 °C form anisotropic polymer aggregates on cooling the sample into the H_1 phase (see, for example, Figure 4h at 25 °C). The H_1 texture observed is much finer, when compared with the sample at pH = 5, suggesting smaller domain dimensions at pH = 1. On further cooling the pH = 1 sample to 10 °C, we observe that there is no qualitative change in the structure of the anisotropic PEI precipitates, however, there is higher optical contrast relative to that at 25 °C, Figure 4j,k.

We summarize the results from our visual observations, SAXs, and optical microscopy on a pH−temperature "state diagram" (Figure 5). Clearly, the H_1 phase forms at lower temperatures as we increase pH from 1 to 12.8. For the samples at pH = 12.8, the samples are always clear, and we always see a coexistence of isotropic micellar and H_1 phases, even at the lowest temperature (10 °C). At pH = 5, the sample gels to form the H_1 phase, and

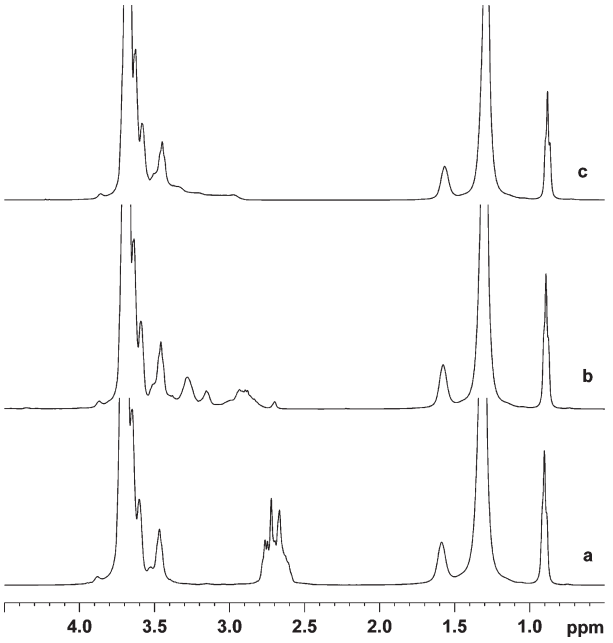

Figure 6. ^{1}H NMR of 5 wt % PEI in 25 wt % $C_{12}E_9/D_2O$ at (a) pH 12.8, (b) pH 5, and (c) pH 1.

then turns opaque as the PEI chains phase separate and aggregate at the H_1 domain boundaries. Finally, at pH = 1, there is phase separation of the PEI chains from the isotropic micellar solution at about 28 °C, resulting in turbidity, followed by formation of the H_1 phase on cooling to about 26 °C. We also indicate the temperature at which the gel can support its own weight in a 5 mL vial (viz., when the yield stress exceeds $1/2\ \rho g r \approx 3.5$ kPa, where ρ is the density of the sample, g is the acceleration due to gravity and r is the radius of the vial). We observe that the sample forms a gel stiff enough to support its weight with the onset of the formation of the H_1 phase. Thus, the PEI decreases the T_{HI} of the surfactant/H_2O system at all pH values, relative to the neat H_1 phase, and this decrease is more pronounced at higher pH. Our data points to pH-dependent interactions between the PEI and the nonionic surfactant, with stronger interactions at higher pH, that suppress the formation of the H_1 phase to lower temperatures compared with the neat $C_{12}E_9/H_2O$ system. We now describe NMR experiments that probe these interactions in detail.

NMR Studies. *(a). ^{1}H NMR.* We obtained ^{1}H NMR of samples containing 5% PEI and 25 wt % $C_{12}E_9$ in D_2O (Figure 6). At these surfactant concentrations, we do not observe the formation of an H_1 phase at room temperature, where NMR was performed. Thus, the samples are in a low viscosity isotropic micellar phase for all the NMR experiments reported here. We observe that there is no change in the position of the peaks from methylene protons in PEI at different pH due to the presence of the nonionic surfactant (compare Figure 6 with Figure 1). In addition to the peaks from the PEI, we observe peaks at δ = 3.3−3.75 ppm corresponding to protons in the ethylene oxide, -(OCH_2-CH_2-O)- units in the surfactant and, at δ = 0.75−1.5 ppm corresponding to the methyl, -CH_3, and methylene protons, -CH_2-, in the hydrophobic surfactant tail. At pH = 12.8, the -CH_2- protons from PEI and the ethylene oxide proton peaks are well separated and can be easily distinguished (Figure 6a). However, for pH = 5 and 1, as the PEI -CH_2- peaks shift downfield (Figures 1 and 6b,c), they overlap with the peaks from the ethylene oxide units in the surfactant and are difficult to distinguish (especially for pH = 1, Figure 6b,c).

(b). 2-D NMR (ROESY Experiments). We employ 2D ROESY to probe surfactant−PEI−water interactions. This experiment uses Nuclear Overhauser Enhancement (NOE) to probe the spatial proximity of protons, for systems in the long correlation limit. ROESY data for the PEI/$C_{12}E_9/H_2O$ systems at pH = 1, 5, and 12.8 is shown in Figure 7. In all the cases, cross-peaks within the surfactant system, that is, between the ethylene glycol moieties and aliphatic protons of the C_{12} moieties could be clearly seen, indicating the micellar nature of the surfactant. Since $C_{12}E_9$ remains in the micellar form at all experimental pH values, their cross peak intensities are similar, to a first approximation. At pH 12.8 (Figure 7a), we can clearly observe cross peaks between the methylene protons, -CH_2-, of the PEI (δ = 2.6−2.7) and protons in the -OCH_2- groups (δ = 3.6) of the surfactant, suggesting spatial proximity between the PEI and hydrophilic units of the surfactant. At pH = 12.8, we also observe cross peaks that indicate spatial proximity between water (δ = 4.7) and the -OCH_2- groups of the surfactant and the -CH_2- group of PEI. As the pH is decreased, we observe a decrease in the intensity of the cross peaks from the surfactant -OCH_2- protons and the PEI protons, indicating a decrease in the surfactant-PEI interactions. At pH = 5 and 1, ROESY cross peaks are either very weak relative to those at pH = 12.8 or are absent (Figure 7b,c). The complete ROESY spectra have been shown in the Supporting Information, Figure S7.

Thus, the NMR data confirms that there are interactions between the PEI and surfactant, that result in their spatial proximity, and in accord with our other data, indicates that the magnitude of PEI-surfactant interactions decreases with decrease in pH. We now, use molecular dynamics simulations to understand the influence of pH on the chain conformations of the PEI and to probe PEI-surfactant interactions at atomistic level. We begin by modeling the behavior of PEI chains in water, at various levels of protonation, to understand the effect of changing pH. Subsequently, we examine a system containing PEI (at different levels of protonation) and surfactant molecules in water to compare with the experimental data.

Computer Simulations. *(a). Single Linear PEI Chain (20- and 50-mer) in Water.* To investigate the size and shape of PEI chain as a function of ionization along the chain, we did all atom molecular dynamic simulations for a single chain in water. Simulations were carried out on a linear PEI chain containing 20 and 50 monomer units of -(CH_2-CH_2-NH)- (in comparison, the number of monomer units for the 2000 g/mol^{-1} PEI used in the experiments is ∼43, and our NMR data indicates the presence of chain branching). We performed simulations for 50 ns, and the last 10 ns of the trajectory was used for analysis of the end-to-end distance and the radius of gyration (R_g) to understand the effect of protonation on the size and the shape of the polymer chain. For the all-protonated system, the end-to-end distance and the radius of gyration (R_g) are greater than that of the alternate-protonated and unprotonated systems (Figure 8 and Table 1). The snapshots, created using PyMol[46] for the PEI chain at different levels of protonation are shown in Figure 8. Clearly, the PEI chain expands due to repulsion between the charged amine groups as the pH is reduced. The end-to-end distance and R_g for the unprotonated 20-mer chain is in agreement with the calculations reported by Zakharova et al.[45]

We have also computed the radial distribution functions for all possible nearest neighbor (NN) as well as next nearest neighbor (NNN) nitrogen atoms present in the 20- and 50-mer PEI chains, by averaging over 50 ns of the simulation trajectory. We

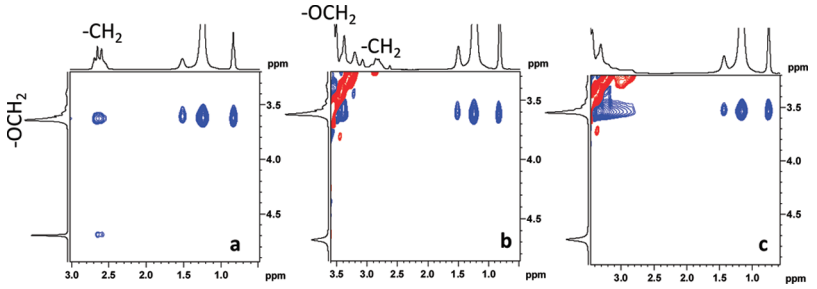

Figure 7. 2D ROESY spectrum for 5 wt % PEI in 25 wt % $C_{12}E_9$ in D_2O at (a) pH 12.8, (b) pH 5, and (c) pH 1.

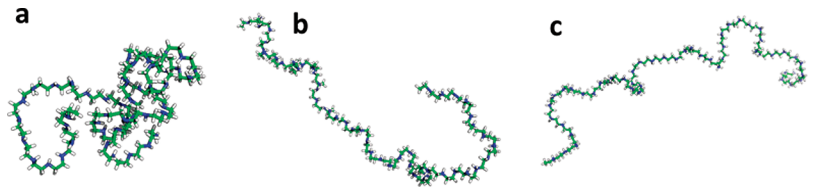

Figure 8. Snapshots of 50-mer linear PEI chain at different levels of protonation: (a) no protonation, (b) alternate protonation, (c) all protonation.

note that the NN and NNN distribution for the 20-mer chains are in quantitative agreement with Ziebarth et al.[33] (Supporting Information, Figure S8). For the 50-mer chains, the NN distribution (Figure 9a) exhibits two prominent peaks at 0.29 and 0.38 nm, for both unprotonated and alternate-protonated chains. The all-protonated state also exhibits two peaks, with a weak peak at 0.32 nm and a stronger peak at 0.38 nm. These peaks correspond to the syn- and anti-conformation, respectively (Table 2), suggesting that, in the all-protonated system, the neighboring nitrogen atoms are mostly anti. For the NNN distribution (Figure 9b), we observe five peaks for the unprotonated chain (at 0.45, 0.50, 0.57, 0.66, and 0.73 nm) and three for alternate protonation (at 0.47, 0.56, and 0.65 nm). For the all-protonated chain, we observe three peaks (at 0.61, 0.68, and 0.74 nm). The syn−syn, syn−anti, and anti−anti configurations (Table 2c−e) correspond to distances of ∼0.57, ∼0.95, and ∼0.73 nm, respectively. The NNN distributions and the NN distributions at different levels of protonation for the 50-mer are in accord with the 20-mer (data for 20-mer chain are in Supporting Information, Figure S8).

(b). PEI Chains with Surfactant Molecules. Simulations of the nonionic surfactant H_1 mesophase are computationally very expensive. Therefore, to understand surfactant−PEI interactions, we simulate a system having 10 PEI chains and 49 surfactant molecules, solvated with TIP3P water molecules. We performed 100 ns simulations, for both the nonprotonated PEI and all protonated PEI systems with surfactants, and the trajectory for the last 10 ns has been analyzed. Figure 10a,b, created using PyMol,[46] clearly depicts the differences in interaction of the all protonated (Figure 10b) and unprotonated (Figure 10a) PEI chains with the surfactant. In Figure 10, the water molecules are not shown for clarity. The surfactant self-assembles with its nonpolar tail buried inside, shielded from the water molecules by the polar head groups. To check the interaction between the surfactant molecules and the PEI chains, we plotted the pair distribution between the oxygen atoms of the surfactants and nitrogen atoms of the PEI chains (Figure 11). The minima for the first peak for both the fully protonated and unprotonated cases are at 0.36 nm. We find a higher value of the peak for the unprotonated system, indicating that this system has higher attractive interactions between the PEI and the surfactant molecules, as compared to the all protonated system. We observe that integrating the first peak for the unprotonated system yields a 10-fold higher peak area compared with the all protonated system. This result is in good accord with the experimental NMR observations. Finally, we also note that, for unprotonated PEI, a comparison of pair distribution functions for nitrogen atoms on the PEI with the oxygen atoms on the surfactant (indicative of dipolar interactions, Figure 11), with carbon atoms present in the PEI chain and carbon atoms in the hydrophobic part of the surfactant (indicative of hydrophobic interactions, Supporting Information) clearly indicates that PEI−surfactant interactions are dominated by hydrophobic interactions.

Table 1. Values for the Size of PEI Chains as a Function of Protonation Along the Linear PEI Chain of 20- and 50-mer Lengths

	unprotonated (nm)	alternate protonated (nm)	all protonated (nm)
		20-mer	
end-to-end distance	2.37 ± 0.82	3.83 ± 0.56	5.38 ± 0.56
radius of gyration (R_g)	0.97 ± 0.16	1.27 ± 0.56	1.79 ± 0.74
		50-mer	
end-to-end distance	3.25 ± 0.77	6.77 ± 1.34	8.45 ± 1.23
radius of gyration (R_g)	1.23 ± 0.12	2.41 ± 0.25	2.76 ± 0.18

Comparison of Experimental Data with Simulations. Nonionic surfactants, such as $C_{12}E_9$ used in our work, typically interact weakly with water-soluble polymers, when compared with ionic surfactants. In previous work on PNIPAM in a $C_{12}E_9/H_2O$ system,[7] we observed very little influence of the polymer on the surfactant phase behavior. However, for the system investigated here, we observe that the presence of PEI strongly influences the $C_{12}E_9/H_2O$ phase transition temperatures and,

dx.doi.org/10.1021/jp202614x |J. Phys. Chem. B 2011, 115, 9059–9069

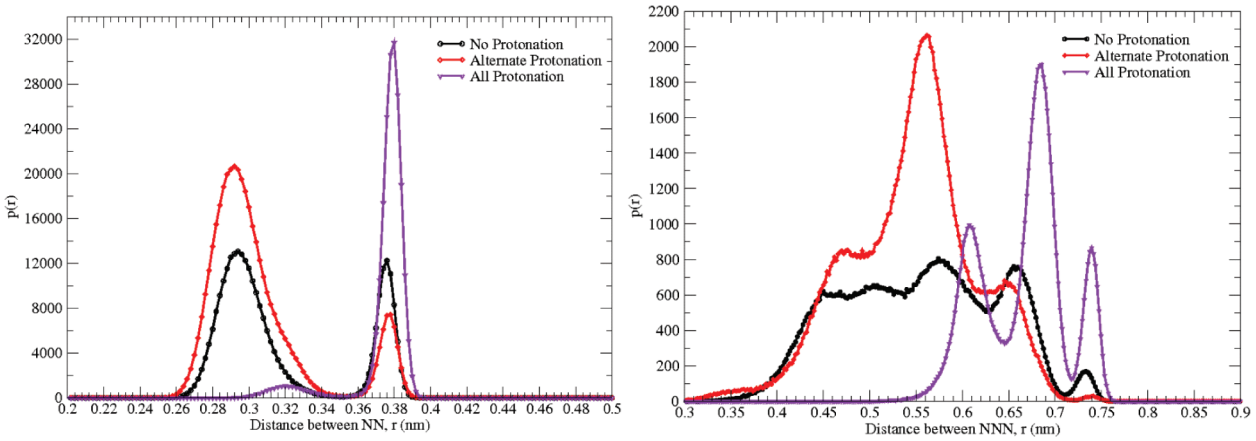

Figure 9. Radial distribution plots of 50-mer PEI chain in water: (a) nearest neighbor (NN) and (b) next nearest neighbor (NNN) distribution.

Table 2. Conformations of Hydrogen Atoms Connected To Amino Groups of PEI Chain

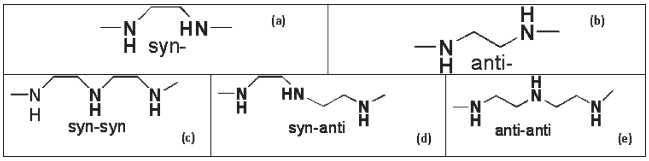

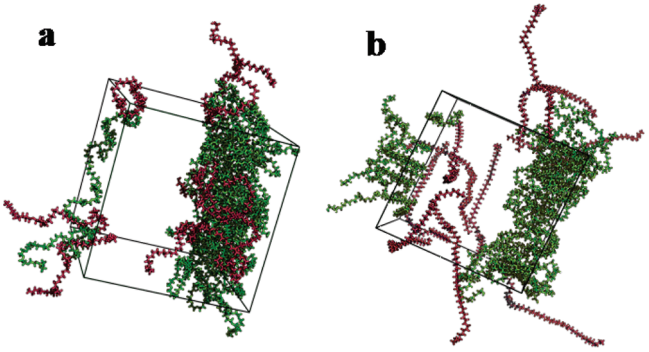

Figure 10. PEI−water−surfactant system containing 10 PEI chain and 49 surfactant molecules: (a) unprotonated; (b) all protonated. It can be clearly seen that the PEI chains do not interact with the surfactant in the all protonated case. The surfactant molecules are shown as green and the PEI is presented in violet as a ball and stick model.

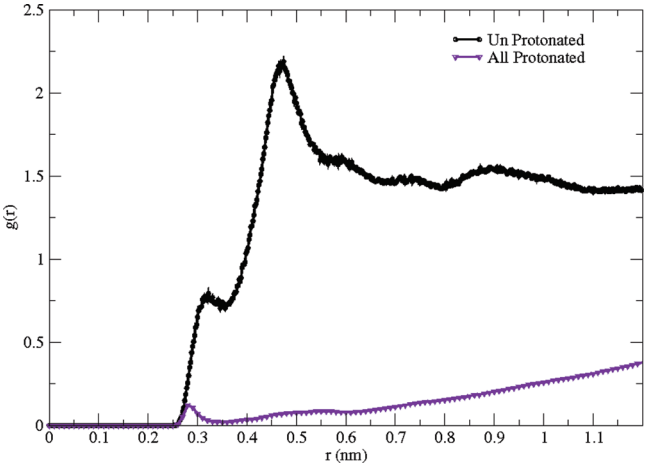

Figure 11. Pair distribution between all the nitrogen atoms present in the PEI chain−all protonated and no-protonated system and all the oxygen atoms present in the surfactant molecules.

further, that this effect of PEI is a strong function of pH. Because pH does not significantly affect the phase behavior of the neat $C_{12}E_9/H_2O$ phase, it is clear that the change in PEI−surfactant interactions with pH influences the isotropic−H_1 transition in the $C_{12}E_9/H_2O$ system. Our NMR data and simulations point to a change in the PEI−surfactant microstructure with change in pH. We observe higher spatial proximity between the PEI and the hydrophilic units of the surfactant at pH = 12.8, as compared to lower pH (= 5, 1). With a decrease in pH, we expect higher protonation of the PEI, as indicated by NMR (Figure 1). With an increase in protonation, our simulations reveal an increase in the end-to-end distance of the PEI chain, as expected. Our simulations also accord with the NMR data on the aqueous PEI/surfactant systems and indicate that the PEI−surfactant interactions are higher when the PEI is not protonated. This interaction between the PEI and the surfactant inhibits formation of the H_1 phase. Our simulations indicate that the protonated PEI goes to solution phase more easily than unprotonated PEI, because the solvation energy of protonated PEI overrides the interaction energy with surfactant molecules. For protonated PEI, we observe an extended chain structure, allowing the water to access the chain more than for the unprotonated PEI. Thus, the protonated PEI gains solvation energy.

At pH = 12.8, the strong PEI−surfactant interaction results in coexistence of the H_1 phase with the isotropic micellar phase, even when the sample is cooled to 10 °C. In fact, even when this sample is cooled to lower temperatures, ≈5 °C, the sample remains a clear gel and there is a coexistence of the H_1 and

dx.doi.org/10.1021/jp202614x |J. Phys. Chem. B 2011, 115, 9059–9069

isotropic micellar phases. For pH = 5, the formation of the H_1 phase on cooling results in the expulsion of PEI to aggregated particles. As in the case of the PNIPAM,[7] the phase separation of PEI appears to result from H_1 phase formation. At surfactant concentrations (<35%) where the H_1 phase does not form, the PEI stays in solution in the isotropic micellar phase, even on cooling to lower temperature (10 °C). Thus, the H_1 phase forms at higher temperatures relative to pH = 12.8, due to the decrease in PEI−surfactant interactions, and once the H_1 phase forms, the PEI chains cannot be localized within the H_1 domains and are expelled to the domain boundaries. On decreasing the temperature further (to 10 °C), the fraction of the isotropic micellar phase decreases relative to the H_1 phase, and the PEI aggregates are dehydrated, forming increasingly optically dense structures at the H_1 domain boundaries. At the lowest pH (= 1), a further decrease in PEI−surfactant interactions relative to pH = 5 results in expulsion of the PEI into polymer-rich droplets, even while the surfactant is in the isotropic micellar phase. After the PEI is expelled, the surfactant/water system forms an H_1 phase, and anisotropic PEI aggregates are observed. At this low pH, we expect that the PEI is in an extended conformation relative to pH = 12.8 and that the PEI chains are protonated. It is interesting that the formation of the H_1 phase by the surfactant/water system results in aggregation of protonated PEI chains by expulsion to the H_1 domain phase boundaries. It is not currently clear how the protonation, and the increase in the chain end-to-end distance results in the formation of anisotropic aggregates. It is possible that correlations between the charges on the protonated chains and in the counterions in solution results in the observed anisotropic aggregates.

SUMMARY

We demonstrate the pH dependence of structuration in a PEI/$C_{12}E_9$/H_2O system. The $C_{12}E_9$/H_2O system is not influenced by pH. However, on addition of PEI, pH-dependent PEI−surfactant interactions influence the transition from the isotropic to H_1 phase. At high pH (=12.8), the transition to the H_1 phase is significantly suppressed to lower temperatures, from 50 °C for the neat $C_{12}E_9$/H_2O system to 13 °C for the system containing 5% PEI. Even at low temperatures, when the H_1 phase forms, strong PEI−$C_{12}E_9$ interactions result in a coexistence of the H_1 phase with an isotropic micellar phase. Thus, a clear gel is obtained for the PEI/$C_{12}E_9$/H_2O system at high pH, even at low temperatures. In contrast, for lower pH (= 5, 1), we observe higher T_{HI} relative to pH = 12.8. On cooling, the $C_{12}E_9$/H_2O system organizes into the H_1 phase, and the formation of the organized mesophase expels the PEI to the mesophase domain boundaries. Competition to complex with water results in dehydration of the PEI below T_{HI}, and therefore, the PEI aggregates at the H_1 domain boundaries form structures that are observed as optically dense structures that scatter light and render the gel turbid. Molecular dynamics simulations confirm that protonated linear PEI chains (representative of the low pH state) interact less strongly with the nonionic surfactant, when compared with unprotonated chains (representative of the high pH state). The protonated chains are extended relative to the unprotonated chains, thus, possibly explaining the formation of anisotropic PEI aggregates below T_{HI} for pH = 1.

ASSOCIATED CONTENT

Supporting Information. TLC and HPLC data of surfactant, SAXs of neat H_1 phase at different pH, specific viscosity data for PEI solutions, snapshots of samples at different pH and temperature, optical micrographs, and NMR and detailed simulation data. This material is available free of charge via the Internet at http://pubs.acs.org.

AUTHOR INFORMATION

Corresponding Author

*Tel.: 91-20-2590-2182. Fax: 91-20-2590-2618. E-mail: g.kumaraswamy@ncl.res.in.

ACKNOWLEDGMENT

We gratefully acknowledge help from Dr. C. V. Avadhani, Ms. Nilakshi Sadavate, and Mr. Mayur Dhaygude for carrying out HPLC experiments to characterize the surfactant.

REFERENCES

(1) (a) Drummond, C. J.; Fong, C. *Curr. Opin. Colloid Interface Sci.* **2000**, *4*, 449–456. (b) Farkas, E.; Zelkó, R.; Németh, Z.; Pálinkás, J.; Marton, S.; Rácz, I. *Int. J. Pharm.* **2000**, *193*, 239–245. (c) Clogston, J.; Caffrey, M. *J. Controlled Release* **2005**, *107*, 97–111. (d) Mohammady, S. Z.; Pouzot, M.; Mezzenga, R. *Biophys. J.* **2009**, *96*, 1537–1546. (e) Shah, J. C.; Sadhale, Y.; Chilukuri, D. M. *Adv. Drug Delivery Rev.* **2001**, *47*, 229–250. (f) Koltover, I.; Salditt, T.; Radler, J. O.; Safinya, C. R. *Science* **1998**, *281* (5373), 78–81. (g) Radler, J. O.; Koltover, I.; Salditt, T.; Safinya, C. R. *Science* **1997**, *275* (5301), 810–814. (h) Safinya, C. R.; Ewert, K.; Ahmad, A.; Evans, H. M.; Raviv, U.; Needleman, D. J.; Lin, A. J.; Slack, N. L.; George, C.; Samuel, C. E. *Philos. Trans. R. Soc., A* **2006**, *364* (1847), 2573–2596.

(2) (a) Mezzenga, R.; Schurtenberger, P.; Burbidge, A.; Michel, M. *Nat. Mater.* **2005**, *4*, 729–740. (b) Ubbink, J.; Burbidge, A.; Mezzenga, R. *Soft Matter* **2008**, *4*, 1569–1581.

(3) Twaites, B. R.; de las Heras Alarcón, C.; Cunliffe, D.; Lavigne, M.; Pennadam, S.; Smith, J. R.; Górecki, D. C.; Alexander, C. *J. Controlled Release* **2004**, *97* (3), 551–566.

(4) Park, I.-K.; Singha, K.; Arote, R. B.; Choi, Y.-J.; Kim, W. J.; Cho, C.-S. *Macromol. Rapid Commun.* **2010**, *31* (13), 1122–1133.

(5) Sethuraman, V. A.; Na, K.; Bae, Y. H. *Biomacromolecules* **2005**, *7* (1), 64–70.

(6) Werth, S.; Urban-Klein, B.; Dai, L.; Höbel, S.; Grzelinski, M.; Bakowsky, U.; Czubayko, F.; Aigner, A. *J. Controlled Release* **2006**, *112* (2), 257–270.

(7) Jijo, V. J.; Sharma, K. P.; Mathew, R.; Kamble, S. B.; Rajamohanan, P. R.; Ajithkumar, T. G.; Badiger, M. V.; Kumaraswamy, G. *Macromolecules* **2010**, *43*, 4782–4790.

(8) Holmberg, K.; Jönsson, B.; Kronberg, B.; Lindman, B. *Surfactants and Polymers in Aqueous Solution*, 2nd ed.; John Wiley and Sons: West Sussex, U.K., 2003.

(9) (a) Goddard, E. D. *Colloids Surf.* **1986**, *19*, 301–329. (b) Antonietti, M.; Conrad, J.; Thuenemann, A. *Macromolecules* **1994**, *27* (21), 6007–6011. (c) Faul, C.; Antonietti, M.; Sanderson, R.; Hentze, H. -P. *Langmuir* **2001**, *17* (6), 2031–2035. (d) von Ferber, C.; Lowen, H. *Faraday Discuss* **2005**, *128*, 389–405. (e) Hentze, H. -P. *Dekker Encyclopedia of Nanoscience and Nanotechnology*, 2nd ed.; CRC: New York, 2009; pp 3403−3408. (f) Thünemann, A. F. *Prog. Polym. Sci.* **2002**, *27* (8), 1473–1572.

(10) Iliopoulos, I.; Wang, T. K.; Audebert, R. *Langmuir* **1991**, *7* (4), 617–619.

(11) Saito, S. In *Nonionic Surfactants: Physical Chemistry*; Schick, M. J., Ed.; Marcel Dekker: New York, 1987; pp 881−926.

(12) Magny, B.; Iliopoulos, I.; Audebert, R.; Piculell, L.; Lindman, B. *Prog. Colloid Polym. Sci.* **1992**, *89*, 118–121.

(13) Bystryak, S. M.; Winnik, M. A.; Siddiqui, J. *Langmuir* **1999**, *15* (11), 3748–3751.

(14) Winnik, M. A.; Bystryak, S. M.; Chassenieux, C.; Strashko, V.; Macdonald, P. M.; Siddiqui, J. *Langmuir* **2000**, *16* (10), 4495–4510.
(15) Wang, H.; Wang, Y.; Yan, H.; Zhang, J.; Thomas, R. K. *Langmuir* **2006**, *22* (4), 1526–1533.
(16) Gainanova, G.; Zhil'tsova, E.; Kudryavtseva, L.; Lukashenko, S.; Timosheva, A.; Kataev, V.; Konovalov, A. *Colloid J.* **2006**, *68* (5), 533–540.
(17) Kotz, J.; Kosmella, S. *Curr. Opin. Colloid Interface Sci.* **1999**, *4*, 348–353.
(18) (a) Ligoure, C.; Bouglet, G.; Porte, G. *Phys. Rev. Lett.* **1993**, *71* (21), 3600–3603. (b) Singh, M.; Ober, R.; Kleman, M. *J. Phys. Chem.* **1993**, *97* (42), 11108–11114. (c) Ligoure, C.; Bouglet, G.; Porte, G.; Diat, O. *J. Phys. II* **1997**, *7*, 473–491. (d) Zhang, K.; Linse, P. *J. Phys. Chem.* **1995**, *99*, 9130–9135.
(19) (a) Radlinska, E. Z.; Gulik-Krzywicki, T.; Lafuma, F.; Langevin, D.; Urbach, W.; Williams, C. E.; Ober, R. *Phys. Rev. Lett.* **1995**, *74* (21), 4237–4241. (b) Radlinska, E. Z.; Gulik-Krzywicki, T.; Lafuma, F.; Langevin, D.; Urbach, W.; Williams, C. E. *J. Phys. II* **1997**, *7*, 1393–1416.
(20) Kekicheff, P.; Cabane, B.; Rawiso, M. *J. Colloid Interface Sci.* **1984**, *102* (1), 51–70.
(21) (a) Iliopoulos, I.; Olsson, U. *J. Phys. Chem.* **1994**, *98*, 1500–1505. (b) Ficheux, M.-F.; Bellocq, A.-M.; Nallet, F. *J. Phys. II* **1995**, *5*, 823–834. (c) Ficheux, M.-F.; Bellocq, A.-M.; Nallet, F. *Colloid Surf., A* **1997**, *123*, 253–263.
(22) Deme, B.; Dubois, M.; Zemb, T.; Cabane, B. *J. Phys. Chem.* **1996**, *100* (9), 3828–3838.
(23) Pacios, I. E.; Renamayor, C. S.; Horta, A.; Lindman, B.; Thuresson, K. *J. Phys. Chem. B* **2005**, *109* (50), 23896–23904.
(24) Pacios, I. E.; Renamayor, C. S.; Horta, A.; Thuresson, K.; Lindman, B. *Macromolecules* **2005**, *38* (5), 1949–1957.
(25) Ligoure, C.; Bouglet, G.; Porte, G. *Phys. Rev. Lett.* **1993**, *71* (21), 3600–3603.
(26) Yamamoto, J.; Tanaka, H. *Nat. Mater.* **2005**, *4*, 75–80.
(27) Iliopoulos, I.; Olsson, U. *J. Phys. Chem.* **1994**, *98*, 1500–1505.
(28) Yang, Y.; Prud'homme, R.; Richetti, P.; Marques, C. M. *Supramolecular Structure in Confined Geometries*; American Chemical Society: Washington, DC, 1999; Vol. 736, pp 169−179.
(29) Radlinska, E. Z.; Gulik-Krzywicki, T.; Lafuma, F.; Langevin, D.; Urbach, W.; Williams, C. E.; Ober, R. *Phys. Rev. Lett.* **1995**, *74* (21), 4237–4241.
(30) Radlinska, E. Z.; Gulik-Krzywicki, T.; Lafuma, F.; Langevin, D.; Urbach, W.; Williams, C. E. *J. Phys. II* **1997**, *7*, 1393–1416.
(31) Bax, A.; Davis, D. G. *J. Magn. Reson.* **1985**, *63*, 207–213.
(32) (a) van der Spoel, D.; Lindahl, E.; Hess, B.; Broenhof, G. *J. Comput. Chem.* **2005**, *26*, 1701–1718. (b) Lindahl, E.; Van der Spool, D.; Kutzer, C.; Hess, B. *J. Chem. Theory Comput.* **2008**, *4*, 435–447. (c) http://www.gromacs.org.
(33) Ziebarth, J. D.; Wang, Y. *Biomacromolecules* **2010**, *11*, 29–38.
(34) (a) Sorin, E. J.; Pande, V. S. *Biophys. J.* **2005**, *88*, 2472–2493. (b) DePaul, A. J.; Thompson, E. J.; Patel, S. S.; Haldeman, K.; Sorin, E. J. *Nucleic Acids Res.* **2010**, *38*, 4856–4867.
(35) Frisch, M. J.; Trucks,G. W.;Schlegel, H. B.; Scuseria, G. E.; Robb, M. A.; Cheeseman, J. R.; Montgomery, J. A., Jr.; Vreven, T.; Kudin, K. N.; Burant, J. C.; Millam,J. M.; Iyengar, S. S.; Tomasi, J.; Barone, V.; Mennucci, B.; Cossi, M.; Scalmani, G.; Rega, N.; Petersson, G. A.; Nakatsuji, H.; Hada, M.; Ehara, M.; Toyota, K.; Fukuda, R.; Hasegawa, J.; Ishida, M.; Nakajima, T.; Honda, Y.; Kitao, O.; Nakai, H.; Klene, M.; Li, X.; Knox, J. E.; Hratchian, H. P.; Cross, J. B.; Bakken, V.; Adamo, C.; Jaramillo, J.; Gomperts, R.; Stratmann, R. E.; Yazyev, O.; Austin, A. J.; Cammi, R.; Pomelli, C.; Ochterski, J. W.; Ayala, P. Y.; Morokuma, K.; Voth, G. A.; Salvador, P.; Dannenberg, J. J.; Zakrzewski, V. G.; Dapprich, S.; Daniels, A. D.; Strain, M. C.; Farkas, O.; Malick, D. K.; Rabuck, A. D.; Raghavachari, K.; Foresman, J. B.; Ortiz, J. V.; Cui, Q.; Baboul, A. G.; Clifford, S.; Cioslowski, J.; Stefanov, B. B.; Liu, G.; Liashenko, A.; Piskorz, P.; Komaromi, I.; Martin, R. L.; Fox, D. J.; Keith, T.; Al-Laham, M. A.; Peng, C. Y.; Nanayakkara, A.; Challacombe, M.; Gill, P. M. W.; Johnson, B.; Chen, W.; Wong, M. W.; Gonzalez, C.; and Pople, J. A. *Gaussian 03*, Revision C.02; Gaussian, Inc.: Wallingford, CT, 2004.
(36) Breneman, C. M.; Wiberg, K. B. *J. Comput. Chem.* **1990**, *11*, 361–373.
(37) Mahoney, M. W.; Jorgensen, W. L. *J. Chem. Phys.* **2000**, *112*, 8910–8922.
(38) Darden, T.; York, D.; Pedersen, L. *J. Chem. Phys.* **1993**, *98*, 10089–10092.
(39) Berendsen, H. J. C.; Postma, J. P. M.; van Gunsteren, W. F.; DiNola, A.; Haak, J. R. *J. Chem. Phys.* **1984**, *81*, 3684–3690.
(40) Bussi, G.; Donadio, D.; Parrinello, M. *J. Chem. Phys.* **2007**, *126*, 0141011–0141017.
(41) (a) Axelson, D. E.; Blake, S. L. *J. Polym. Sci., Polym. Chem. Ed.* **1985**, *23*, 2507–2525. (b) Lukovkin, G. M.; Pshezhetsky, V. S.; Murtazaeva, G. A. *Eur. Polym. J.* **1973**, *9*, 559–565.
(42) Idris, S. A.; Mkhatresh, O. A.; Heatley, F. *Polym. Int.* **2006**, *55*, 1040–1048.
(43) Li, Y.; Ghoreishi, J.; Warr, J.; Bloor, D. M.; Holzwarth, J. F.; Wyn-Jones, E. *Langmuir* **2000**, *16*, 3093–3100.
(44) Sharma, K. P.; Kumaraswamy, G.; Ly., I.; Mondain-Monval, O. *J. Phys. Chem. B* **2009**, *113* (11), 3423–3430.
(45) Zakharova, L. Y.; Ibragimova, A. R.; Valeeva, F. G.; Zakharova, A. V.; Mustafina, A. R.; Kudryavtseva, L. A.; Harlampidi, H. E.; Konovalov, A. I. *Langmuir* **2007**, *23*, 3214–3224.
(46) *The PyMol Molecular Graphics System*, Version 1.3; Schrödinger, LLC: New York, 2010.